Computational and Structural Biotechnology Journal 21 (2023) 2621–2630

Contents lists available at ScienceDirect

Computational and Structural Biotechnology Journal

journal homepage: www.elsevier.com/locate/csbj

Research article

A five-protein prognostic signature with GBP2 functioning in immune cell infiltration of clear cell renal cell carcinoma

Kun Meng [a,b,1], Yu-Ying Li [b,1], Dan-Ya Liu [b], Li-Ling Hu [b], Yun-Long Pan [a,*], Chris Zhiyi Zhang [b,*], Qing-Yu He [a,b,**]

[a] The First Affiliated Hospital of Jinan University, Jinan University, Guangzhou 510632, China
[b] MOE Key Laboratory of Tumor Molecular Biology and Key Laboratory of Functional Protein Research of Guangdong Higher Education Institutes, Institute of Life and Health Engineering, College of Life Science and Technology, Jinan University, Guangzhou 510632, China

ARTICLE INFO

Article history:
Received 30 November 2022
Received in revised form 16 April 2023
Accepted 16 April 2023
Available online 17 April 2023

Keywords:
GBP2
Clear cell renal cell carcinoma
Prognostic signature
Immune-cell infiltration

ABSTRACT

Clear cell renal cell carcinoma (ccRCC) is of poor clinical outcomes, and currently lacks reliable prognostic biomarkers. By analyzing the datasets of the Cancer Genome Atlas (TCGA) and the Clinical Proteomic Tumor Analysis Consortium (CPTAC), we established a five-protein prognostic signature containing GBP2, HLA-DRA, ISG15, ISG20 and ITGAX. Our data indicate that this signature was closely correlated with advanced stage, higher pathological grade, and unfavorable survivals in patients with ccRCC. We further functionally characterized GBP2. Overexpression of GBP2 enhanced the phosphorylation of STAT2 and STAT3 to trigger JAK-STAT signaling and promote cell migration and invasion in ccRCC. Treatment of Ruxolitinib, a specific inhibitor of JAK/STAT, attenuated the GBP2-mediated phenotypes. Patients with high GBP2 expression were accompanied with more infiltration of immune cells positively stained with CD3, CD8, CD68, and immune checkpoint markers PD-1 and CTLA4, which was validated by Opal multiplex immunohistochemistry in ccRCC tissues. More CD8 + T cells and CD68 + macrophages were observed in patients expressing high GBP2. Taken together, a five-protein prognostic signature was constructed in our study. GBP2 has an oncogenic role via modulating JAK-STAT signaling and tumor immune infiltration, and thus may serve as a potential therapeutic target in ccRCC.

1. Introduction

Clear cell renal cell carcinoma (ccRCC) ranks the third most common malignant tumor of the urinary system [1]. More than 15% of ccRCC patients have developed distant metastasis at the time of diagnosis, and the 5-year survival rate of metastatic ccRCC patients is less than 10% [2]. Although promising treatment strategies have significantly improved the clinical outcome of ccRCC, monitoring disease progression remains challenging due to the lack of prognostic factors. Elucidation of the mechanism of tumor initiation and development in ccRCC helps to identify novel prognostic and therapeutic biomarkers [3].

Guanylate-binding proteins 2 (GBP2) belongs to the large GTPases superfamily and is induced by IFN-γ. GBP2 plays an essential role in host natural and autonomous cellular immunity [4] and has been implicated in tumorigenesis [5–8]. For instance, GBP2 inhibited the migration of breast cancer cells [9,10]. In contrast, GBP2 facilitated glioma cell invasion [11,12]. These data highlight the controversial role of GBP2 in cancer metastasis. On the other hand, GBP2 was implicated in drug resistance and immune cell infiltration [13–15]. However, the functional character of GBP2 in ccRCC remains unclear.

In the present study, we performed bioinformatic analyses on public datasets and constructed a five-protein prognostic signature containing GBP2 in ccRCC. We further characterized the role of GBP2 in ccRCC by demonstrating its capability to promote the migration and invasion of ccRCC cells through JAK/STAT pathway. In addition, we found that GBP2 overexpression was correlated with significant

* Corresponding authors.
** Corresponding author at: The First Affiliated Hospital of Jinan University, Jinan University, Guangzhou 510632, China.
E-mail addresses: tpanyl@jnu.edu.cn (Y.-L. Pan), zhangzy@jnu.edu.cn (C.Z. Zhang), tqyhe@email.jnu.edu.cn (Q.-Y. He).
[1] These authors contributed equally to this study.

https://doi.org/10.1016/j.csbj.2023.04.015

infiltration of CD8 + T lymphocytes and CD68 + macrophages. Our data establish the oncogenic character of GBP2 and provide potential prognostic factors in ccRCC.

2. Material and methods

2.1. Data collection

The proteomic dataset was downloaded from the Clinical Proteome Tumor Analysis Consortium (CPTAC, https://cptac-data-portal.georgetown.edu/) [16]. The RNA transcriptome dataset and the corresponding ccRCC clinical information were downloaded from the Cancer Genome Atlas (TCGA, https://portal.gdc.cancer.gov/) database [17]. The altered proteins with p-value < 0.05 and log2 (fold change) ≥ 1 or ≤ −1 were regarded as significantly differentially expressed proteins (DEPs).

2.2. Weighted gene co-expression network analysis (WGCNA)

WGCNA was employed to construct gene co-expression networks using R software's 'WGCNA' package [18]. DEPs obtained from the proteomic data of the CPTAC cohort were applied to construct gene co-expression networks using the scale independence, and tested the average connectivity degree of different modules with different power values (ranging from 1 to 20). The appropriate power value was determined when the degree independence was above 0.85 with a relatively higher connectivity degree. Then, differently expressed proteins were sorted into different gene modules according to topological overlap matrix (TOM)-based dissimilarities, and identified the module with the highest correlation with clinical characteristics was regarded as the key module.

2.3. Risk model construction

Univariate cox regression analysis and LASSO regression analysis were performed to identify the prognostic signature in the training dataset. The risk score for each ccRCC patient was calculated using the following formula: Risk score = ΣExpression × βi. The expression represents the expression level of each hub gene, while βi represents the coefficient of each hub gene.

2.4. Gene set enrichment analysis (GSEA)

Gene Set Enrichment Analysis (GSEA) was performed via the GSEA software (4.1.0) [19]. The c2.cp.kegg.v7.5.symbols.gmt gene set was selected as the reference gene set. KEGG pathways with significant enrichment results were demonstrated based on NES (Net enrichment score), gene ratio, and P-value. Gene sets with |NES| > 1, NOM p < 0.05 were considered enrichment significant.

2.5. siRNA sequence and transfection

The siRNA sequences: siRNA GBP2-#1: 5′- GCUGAACCCUGAUU UCAUATT-3′; siRNA GBP2-#2: 5′- CCAGUUAAUGGCAGAGCAATT-3′. Lipofectamine 3000 (Invitrogen, Carlsbad) was used to transfect siRNA into ccRCC cells according to the manufacturer's instructions. Western blotting was used to verify the efficiency of siRNA knockdown.

2.6. Cell culture

The human ccRCC cell lines ACHN and 769-P were cultured in DMEM medium (Gibco, Carlsbad) supplemented with 10% fetal bovine serum (Gibco, Carlsbad) and 1% penicillin/streptomycin (Gibco, Carlsbad). All cell lines were authenticated by short tandem repeat profiling.

2.7. Western blot

Cells were lysed in RIPA buffer (50 mmol/L Tris-HCl, 150 mmol/L NaCl, 0.5 mmol/L EDTA, 1% NP40, 10% glycerin), and BCA Protein Assay Kit (Pierce, Waltham) was used for protein quantification. Equal proteins were added in loading buffer and boiled at 100 °C for 10 min, then separated by SDS-PAGE, and transferred to a polyvinylidene difluoride (PVDF) membrane (Bio-Rad, Hercules). After being blocked with 5% defatted milk at room temperature for 1 h, the membrane was incubated at 4 °C overnight with the primary antibodies, including GBP2 (Proteintech, Wuhan), β-actin (Cell Signaling Technology, Boston). STAT1 (Cell Signaling Technology, Boston), STAT2 (Proteintech, Wuhan), STAT3 (Beyotime Biotechnology, Shanghai), Phospho-STAT1 (Tyr701) (Cell Signaling Technology, Boston), Phospho-STAT2 (Tyr690) (Beyotime Biotechnology, Shanghai), Phospho-STAT3 (Tyr705) (Beyotime Biotechnology, Shanghai). After being washed with TBST three times, secondary antibodies (Bio-world, Minnesota) were incubated at room temperature for another 1 h. Target protein bands were detected by Chemiluminescence Western Blotting Substrates (Bio-Rad, Hercules), then scanned by Luminescence Imaging System (Tanon, Shanghai).

2.8. Transwell assay

ACHN and 769-P cells were transfected with indicated treatment and subsequently cultured for 24 h. For the cell migration assay, each group of transfected ACHN and 769-P cells were harvested, and 1×10^4 cells in 100 μL of the serum-free medium were placed in the upper chamber of an insert (pore size, 8 μm) (BD Biosciences, Franklin Lakes). The lower chamber was filled with 600 μL DMEM medium with 10% FBS. For the cell invasion assay, 1×10^4 cells in 100 μL of the serum-free medium were placed in the upper chamber precoated with Matrigel (BD Biosciences, Franklin Lakes). The lower chamber was filled with 600 μL DMEM medium with 10% FBS. After 24 h of incubation, cells were fixed with methanol and stained with 1% crystal violet. Then, cells were removed from the upper chamber of the insert using a cotton swab. After that, five random fields were selected to count the number of cells. Assays were performed in triplicate.

2.9. Protein extraction from FFPE and trypsin digestion

Tissue slices were deparaffinized with xylene and rehydrated by gradient ethanol. SDS lysis buffer (0.3 mmol/L Tris-HCl, 4% SDS, pH 8.0) was add to the tissues for protein extraction and the samples were sonicated at 40% amplitude for a total working time of 2 min with 2 s on and 2 s off. Lysates were then centrifuged at 12,000 g for 30 min to remove the insoluble debris and the supernatant was incubated for 60 min at 99 °C in a heating block to untang the cross-linked proteins. Proteins were digested with trypsin through the FASP method [20].

2.10. Immunohistochemistry

Tissue microarrays (TMA) contained ccRCC tissues and adjacent renal tissues were used to evaluate the expression level of GBP2 based on immunohistochemistry (IHC) staining. Another cohort of TMA contained solid tumor tissues were used to evaluate the immune cell infiltration level. Slides with a thickness of 4 μm were deparaffinized with xylene and rehydrated. Antigen retrieval was performed with the sodium citrate buffer (pH 6.0) in a pressure cooker, boiling for 2.5 min. Then, the sections were treated with 3% hydrogen peroxide to quench endogenous peroxidase activity. After incubation with a blocking buffer to block nonspecific binding, the sections were incubated with primary antibodies overnight at 4 °C. The next day, after three rounds of washing with PBS buffer, the tissue sections were incubated with anti-Rabbit or mouse HRP secondary antibody (PV-6000, Zhongshan Golden Bridge Biotechnology, Beijing) for 20 min, followed by washing with

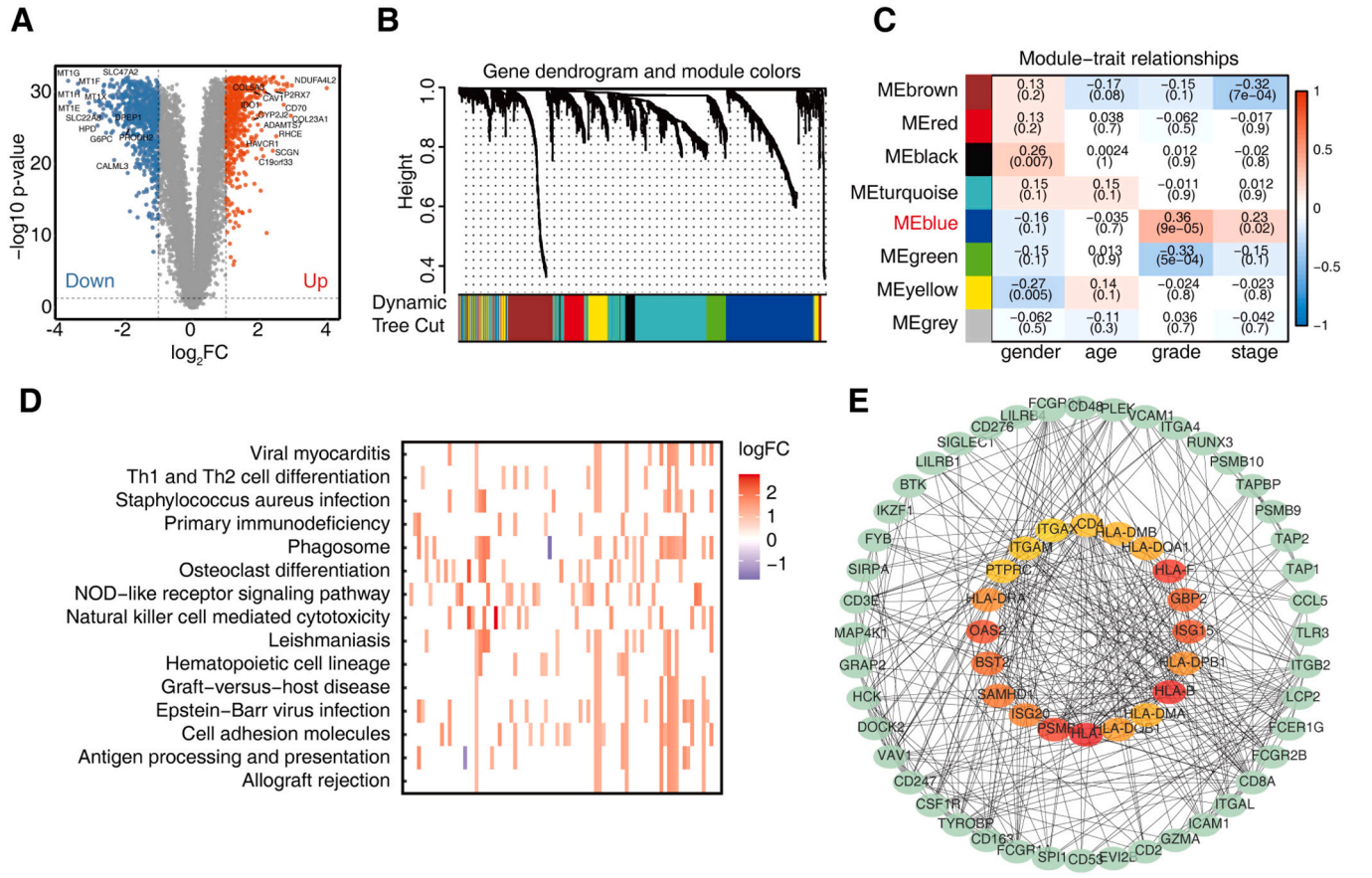

Fig. 1. Weighted co-expression network construction and identification of key modules. A. Volcano plot was drawn to indicate the differentially expressed proteins (DEPs) in ccRCC, comparing with normal tissues. DEPs, |log FC|= ≥ 1 and p < 0.05. Red dots, significantly upregulated proteins. Blue dots, significantly downregulated proteins. Grey dots, non-significantly changed proteins. B. Dendrogram of all differentially expressed proteins clustered based on dissimilarity measurement (1-TOM) was shown. The color bands represent the results obtained from the automatic single-block analyses. C. Gene co-expression modules correlated with clinical characteristics were identified by WGCNA. The blue module was significantly positively associated with the stage and grade of ccRCC. D. KEGG enrichment analysis showed that the proteins in the blue module were significantly enriched in immune-related functional pathways. The columns correspond to proteins enriched in associated pathways. Red columns, upregulated proteins. Blue columns, downregulated proteins. E. Protein-protein interaction (PPI) networks were constructed by Cytoscape software to explore the relationship between the proteins in the blue module. The top 20 hub-genes are represented by a red to yellow gradient.

PBS buffer. DAB chromogen substrate was added to the staining sections, and the staining intensity was observed under the microscope. Two investigators reviewed and scored the immunostaining degree of sections independently, based on the proportion of positively stained cells and the staining intensity.

2.11. Multiplex immunohistochemical staining

Multiplex immunohistochemical staining was conducted using the PANO 5-plex IHC kit (Panovue, Being) to explore the infiltration level of different immune cells in ccRCC. Slides with a thickness of 4 μm were deparaffinized in xylene and rehydrated in ethanol. Antigen retrieval was performed with the EDTA buffer (pH 9.0) by microwave treatment (MWT) for 15 min, and protein blocking was performed using blocking buffer (Panovue, Being). The slides were then incubated with the primary antibodies for 60 min. After that, the slides were washed using TBST buffer and incubated with the HRP-conjugated secondary antibody for 10 min before visualization using fluorophore diluted with tyramide signal amplification (TSA, 1:200 dilution, Panovue, Beijing) for another 10 min. MWT was used to remove the non-covalently bound antibodies. All slides were stained sequentially with the following primary antibodies for CD3 (1:100 dilution, ZM-0428, Zhongshan Golden Bridge) visualized with Opal520 TSA (1:200 dilution), CD8 (1:100 dilution, ZA-0508, Zhongshan Golden Bridge) visualized with Opal570 TSA (1:200 dilution), Cytokeratin (1:100 dilution, ZM-0069, Zhongshan Golden Bridge) visualized with Opal480 TSA (1:200 dilution), and CD68 (1:100 dilution, ZM-0464 Zhongshan Golden Bridge) visualized with Opal780 TSA (1:200 dilution). TSA-stained slides were finished with MWT, counterstained with DAPI for 10 min, and coverslipped using the mounting media. Finally, the sections were imaged using the Vectra Polaris Automated Pathology Imaging platform (Perkin Elmer, Waltham) at 20 x magnification and analyzed using the HALO digital pathology analysis platform (Indica Labs, Corrales).

2.12. Statistical analysis

Graphpad 8.0 and R software (Version 4.1.2) were used for computational and statistical analyses. The Kaplan-Meier curve and log-rank tests determined the survival differences between the high-risk and low-risk groups. For all analyses, P value < 0.05 was considered statistically significant.

3. Results

3.1. Identification of significant differentially expressed proteins in ccRCC

We firstly analyzed the proteomic data of 110 ccRCC patients in CPTAC to identify differentially expressed proteins (DEPs). Compared

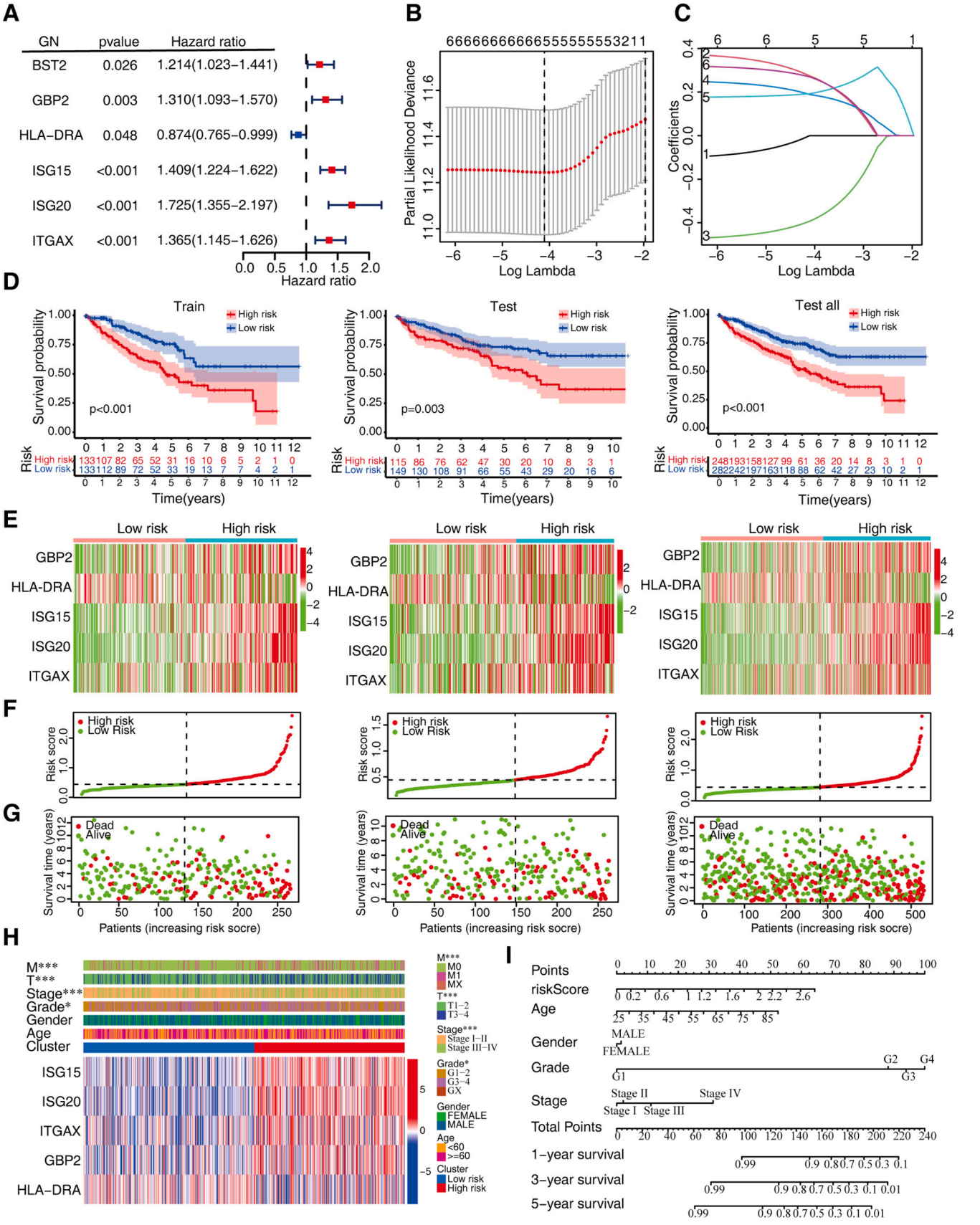

(caption on next page)

Fig. 2. Construction of a prognostic signature for ccRCC patients. A. The univariate Cox regression analysis was performed to identify prognostic hub in TCGA database. Six prognostic genes were identified. B-C. Identification of five-gene prognostic signature using LASSO regression. The optimal values of the penalty parameter were determined by cross-validation (B). Lasso regression analysis was performed for the six prognostic genes (C). D. Kaplan-Meier survival analyses were conducted for ccRCC patients with high-risk group (red) and low-risk group (blue) in the training and test sets. ccRCC patients were randomly divided into low-risk and high-risk groups based on the median risk score. E. Heatmap showed the expression of prognostic genes in the low-risk and high-risk groups in the training and testing sets. F. Distribution of patients in the training set and testing set based on the risk score. G. The survival status for each patient in the training and testing sets. Low-risk population, on the left side of the dotted line; high-risk population, on the right side of the dotted line. The green and red dots represent survival and death, respectively. H. Heatmap for the connections between clinicopathologic features and the clusters of risk. From blue to red means increased gene expression. I. Nomogram depicting clinicopathologic features and risk score. For each patient, five lines were drawn upward to verify the points received from the three predictors of the nomogram. The sum of these points situates on the 'Total Points' axis. Then a line is drawn downward to assess the 1-, 3-, and 5-year overall survival of CRC.

to the adjacent normal tissues, 519 up-regulated and 745 down-regulated DEPs in ccRCC were found (Fig. 1A & Supplementary Table 1). We then applied WGCNA algorithm to identify gene modules with similar expression patterns and related phenotypes. Gene modules strongly correlated to cancer were revealed with the optimal conditions of β = 4 (Supplementary Figure 1A-B). Eight co-expression modules that significantly correlated with tumor stage and grade were next identified (Fig. 1B-C). The MEblue module was positively associated with the clinical stage and pathological grade, and was thus selected for further analyses (Fig. 1C & Supplementary Table 2).

KEGG and GO enrichment analyses were conducted to further explore the biological implications of the proteins in the MEblue module. We found that enriched pathways were mainly related to immune-related functional responses, such as Th1 and Th2 cell differentiation, primary immunodeficiency, antigen processing and presentation (Fig. 1D). The most enriched GO terms in biological process (BP), cellular component (CC) and molecular function (MF) were T cell activation, secretory granule membrane and GTPase regulator activity, respectively (Supplementary Figure 1C). The protein-protein interaction (PPI) network of the MEblue module proteins was generated by using CytoHubba of Cytoscape software. A total of 20 hub genes were identified (Fig. 1E).

3.2. A five-protein prognostic signature for patients with ccRCC

To explore the prognostic value of these 20 hub genes, we conducted a univariate COX proportional hazards regression analysis. Expressions of six proteins were significantly correlated with the clinical outcomes of ccRCC patients (Fig. 2A). LASSO regression analysis was performed to avoid overfitting (Fig. 2B-C). Five proteins including GBP2, HLA-DRA, ISG15, ISG20 and ITGAX were found to be

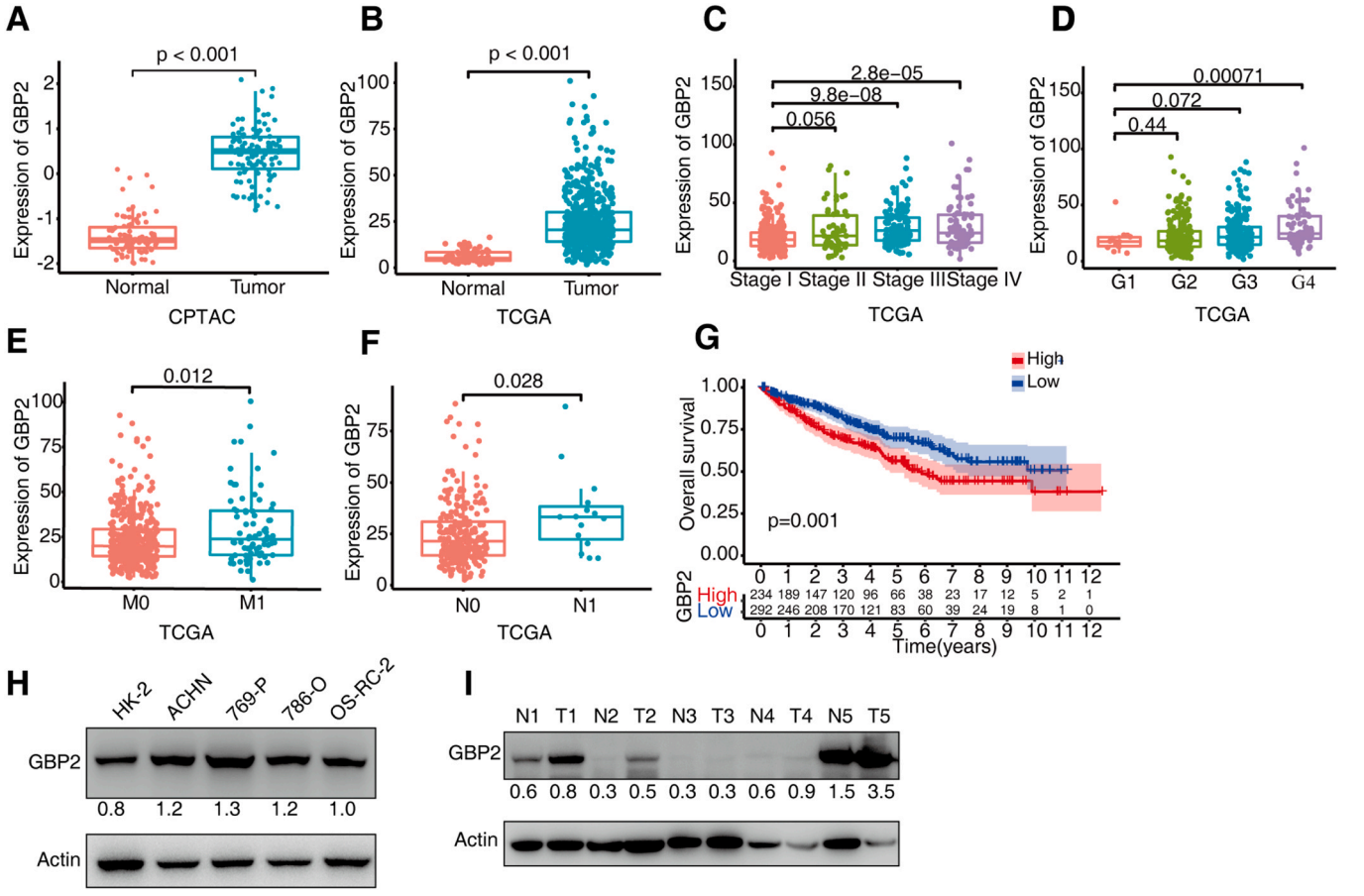

Fig. 3. GBP2 is highly expressed in ccRCC and its high expression is associated with a poor prognosis in ccRCC Patients. A-B. The expression of GBP2 proteins level (A) and RNA level (B) in ccRCC and non-tumor kidney tissues were analyzed in TCGA and CPTAC cohorts. C-D. The expression of GBP2 was compared in ccRCC patients with different stages (C) and different grades (D), using TCGA data. E-F. The expression of GBP2 was compared in ccRCC patients with distant metastasis (E) or lymph node metastasis (F). G. Kaplan-Meier analyses were conducted to indicate the correlation of GBP2 expression and patient survivals. H. The expression of GBP2 was examined in four ccRCC cell lines and normal kidney cell line HK2 by western blotting. The expression of GBP2 was quantified by image J. I. The expression of GBP2 protein was examined in five ccRCC tissues (T) and adjacent non-tumor tissues (N). The expression of GBP2 was quantified by image J.

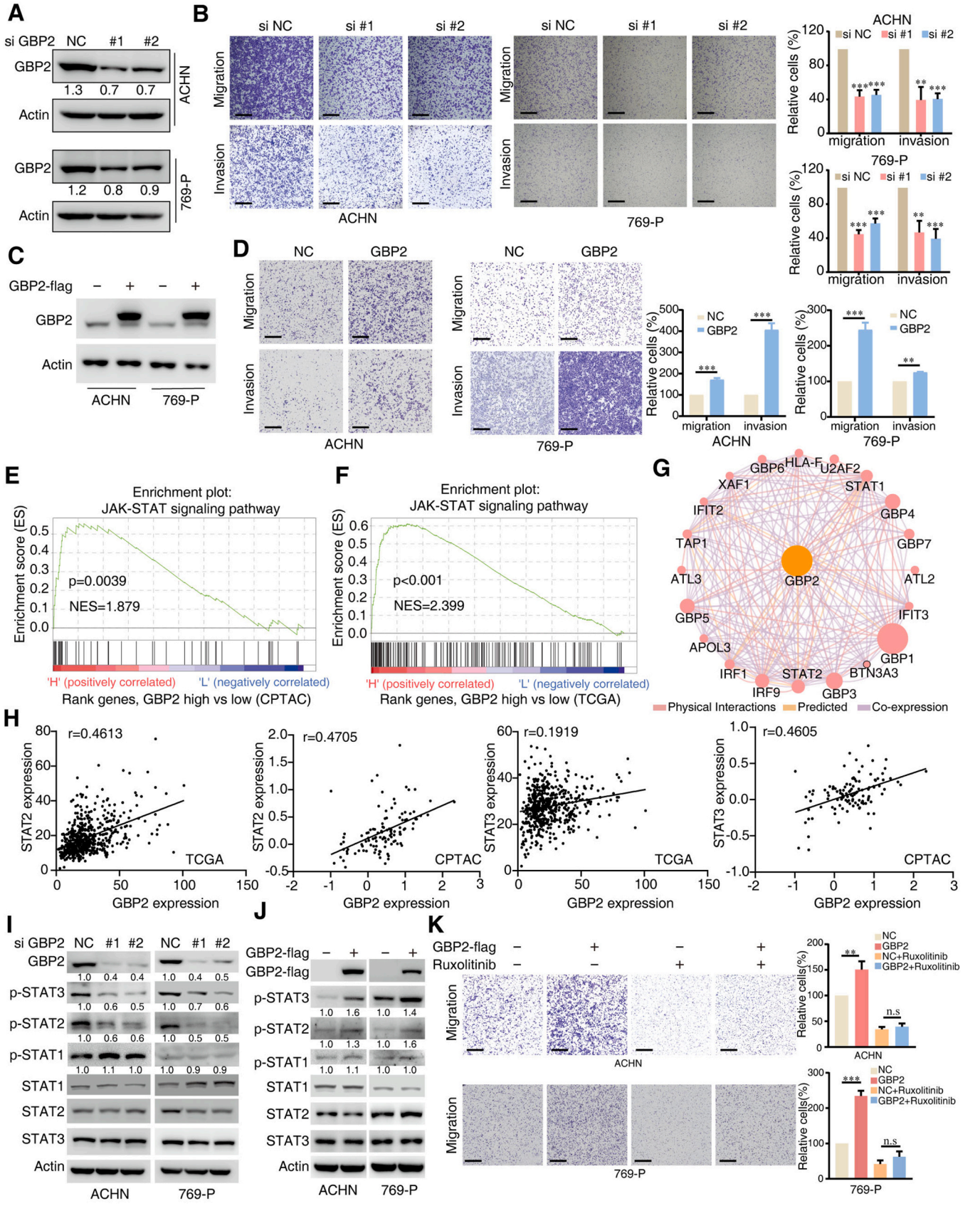

(caption on next page)

Fig. 4. GBP2 enhances metastasis of ccRCC cells through JAK-STAT signaling. A. Western blotting validation of GBP2 expression in ccRCC cells upon knockdown of GBP2. B. Transwell assays were used to test the migration and invasion abilities upon knockdown of GBP2. * *P < 0.01, * **P < 0.001. Scale bar, 600 μm. C. Western blotting validation of GBP2 expression in ccRCC cells transfected with indicated constructs. D. Transwell assays were used to test the migration and invasion abilities of ACHN and 769-P cells transfected with indicated constructs. * *P < 0.01, * **P < 0.001. Scale bar, 600 μm. E-F. Gene Set Enrichment Analysis revealed that high GBP2 expression was mainly enriched in JAK/STAT signaling based on proteome and transcriptome data from CPTAC (E) and TCGA (F). G. Protein-protein interaction network for GBP2 in ccRCC was constructed using GeneMANIA. Different colors of the network edge indicate the bioinformatics methods applied: physical interaction, predicted, and co-expression. H. The correlation of GBP2 with STAT2/STAT3 at both RNA levels (TCGA) and protein levels (CPTAC) in ccRCC was determined. I-J. GBP2 siRNAs (I) or overexpression vectors (J) were transfected into ccRCC cells. The phosphorylation of STAT family proteins was examined by western blotting. K. Transwell assays were used to test the migration abilities of GBP2-expressing ACHN and 769-P cells treated with JAK inhibitor Ruxolitinib. * *P < 0.01, * **P < 0.001. n.s, no significant. Scale bar, 600 μm.

of independent prognostic values in ccRCC, and were therefore submitted for the establishment of a prognostic signature. The risk score of the prognostic signature was calculated by the following formula: Risk Score = (0.27 × GBP2 exp.) + (−0.39 × HLA-DRA exp.) + (0.19 × ISG15 exp.) + (−0.19 × ISG20 exp.) + (0.27 × ITGAX exp.).

To verify the prognostic signature, a total of 530 ccRCC patients from TCGA were randomly divided into training (n = 266) and testing (n = 264) sets. The whole TCGA dataset was also used as another testing set. Patients were divided into high-risk and low-risk groups based on the median risk score. Kaplan-Meier analyses revealed that patients in high-risk group were accompanied with unfavorable survivals in both the training and testing sets (Fig. 2D).

The expressions of the five proteins in the training and testing sets were associated with the prognostic risk in ccRCC (Fig. 2E). More dead cases during post-surgical 5-years were observed in patients with high-risk scores (Fig. 2F&G). Patients with high-risk scores were likely to have higher pathological grade, advanced clinical stage and tumor metastasis (Fig. 2H). Furthermore, the 1–year, 3-year and 5-year survival probabilities were better in patients with lower risk score (Fig. 2I). Taken together, the five-protein signature has prognostic value in ccRCC.

3.3. The high expression of GBP2 in cancers

We next focused on GBP2, one of the five proteins, for further investigation. Dysregulation of GBP2 is frequently observed in tumors [9,11,21]. As shown by Supplementary Figure 2 A, GBP2 mRNA was upregulated in multiple cancers, including glioblastoma multiforme (GBM), renal clear cell carcinoma (KIRC), renal papillary cell carcinoma (KIRP), brain lower grade glioma (LGG), liver hepatocellular carcinoma (LIHC), pancreatic adenocarcinoma (PAAD) and thyroid carcinoma (THCA). Kaplan-Meier analyses showed that high expression of GBP2 was correlated with poor overall survival in KIRC, LGG, PAAD, thymoma (THYM), and uveal melanoma (UVM). In addition, increased GBP2 expression was also associated with unfavorable release-free survival in KIRP, LAML, LGG, and THYM (Supplementary Figure 2B). These findings indicated the prognostic role of GBP2 in cancers. HPA data showed that both nuclear and cytosolic staining of GBP2 were depicted in renal, liver, pancreatic, colorectal, prostate and endometrial cancers (Supplementary Figure 2 C). We next explored the expression and clinical value of GBP2 in ccRCC. Using CPTAC and TCGA databases, we found that GBP2 was significantly up-regulated in ccRCC at both RNA and protein levels, as compared with the adjacent nontumorous tissues (Fig. 3A-B). Overexpression of GBP2 was found in ccRCC patients with higher pathological grade and advanced clinical stage (Fig. 3C-D). In addition, the expression of GBP2 was higher in patients with metastatic ccRCC (Fig. 3E-F). Survival analyses revealed that patients with high GBP2 expression had increased risk of ccRCC-related death (Fig. 3G).

The elevated expression of GBP2 protein in ccRCC was validated in cell lines and clinical fresh specimens. Compared with the expression of GBP2 in immortalized normal human renal HK2 cells, more GBP2 protein was detected in ccRCC cell lines (Fig. 3H). In five pairs of clinical ccRCC samples, GBP2 protein was found to have high expression in tumor (Fig. 3I).

3.4. GBP2 enhances cell migration and invasion in ccRCC

Our data showed that patients with tumor metastasis expressed more GBP2, we next determined whether GBP2 affected cell migration in ccRCC. We knocked down the expression of GBP2 by siRNAs in ACHN and 769-P cells (Fig. 4A). Transwell data demonstrated that GBP2 silence significantly inhibited the migration and invasion of both ACHN and 769-P cells (Fig. 4B). Consistently, overexpression of GBP2 markedly increased migrated and invasive cells in ccRCC (Fig. 4C-D).

GSEA was conducted to investigate the mechanism through which GBP2 exerted pro-metastatic activity. The data suggested that GBP2 was connected with the activation of JAK/STAT signaling (Fig. 4E-F). GeneMANIA [22] presented the PPI network for GBP2, indicating the involvement of GBP2 in JAK/STAT pathway (Fig. 4G). Positive correlation between GBP2 and STAT2/STAT3 was determined using TCGA and CPTAC data in ccRCC (Fig. 4H). Results of western blotting revealed that knockdown of GBP2 suppressed the phosphorylation of STAT2 at Tyr690 and STAT3 at Tyr705 (Fig. 4I). In contrast, the expression levels of phosphorylated STAT2 and phosphorylated STAT3 were increased upon GBP2 overexpression in ccRCC cells (Fig. 4J). Ruxolitinib, a specific inhibitor of JAK, was used to confirm whether GBP2 promoted ccRCC cell migration through JAK/STAT signaling. The results demonstrated that Ruxolitinib effectively attenuated GBP2-mediated cell migration in ACHN and 769-P cells (Fig. 4K). Taken together, these findings suggest that GBP2 promotes cell metastasis in ccRCC via the activation of JAK/STAT pathway.

3.5. GBP2 expression is correlated with immune cell infiltration

GBP2 is involved in the construction of tumor immune microenvironment [14,15]. We collected paraffin-embedded samples from 56 patients with solid tumors and performed proteomic investigation to determine the association of GBP2 with the infiltration of immune cells. Results showed that high expression of GBP2 was associated with more infiltration of immune cells with positive staining of CD3, CD8, CD68, PD1, CTLA4, TIM-3, CD4, FoxP3, CD19, CD86, and CD163 (Fig. 5A & Supplementary Figure 3A). Representative staining results were showed as Fig. 5B and Supplementary Figure 3B. The difference of immune infiltration patterns in ccRCC patients with high or low GBP2 expression was then examined by CIBERSORT algorithm in TCGA cohort. The results showed that high GBP2 expression was associated with more infiltrations of CD8 + cytotoxic T lymphocyte and macrophage (Fig. 5C), two immune cell types that play significant roles in anti-tumor immunity [23,24]. Using multiplex immunohistochemical staining, we further confirmed that patients with high GBP2 expression were accompanied with higher proportion of CD8 + cytotoxic T cells and CD68 + macrophages in ccRCC tissues (Fig. 5D).

4. Discussion

ccRCC, a common malignant tumor in the urinary system, is associated with poor prognosis due to the frequent distant metastasis. Diagnostic and prognostic biomarkers are urgently needed to improve the clinical management of ccRCC. Mass spectrometry-based

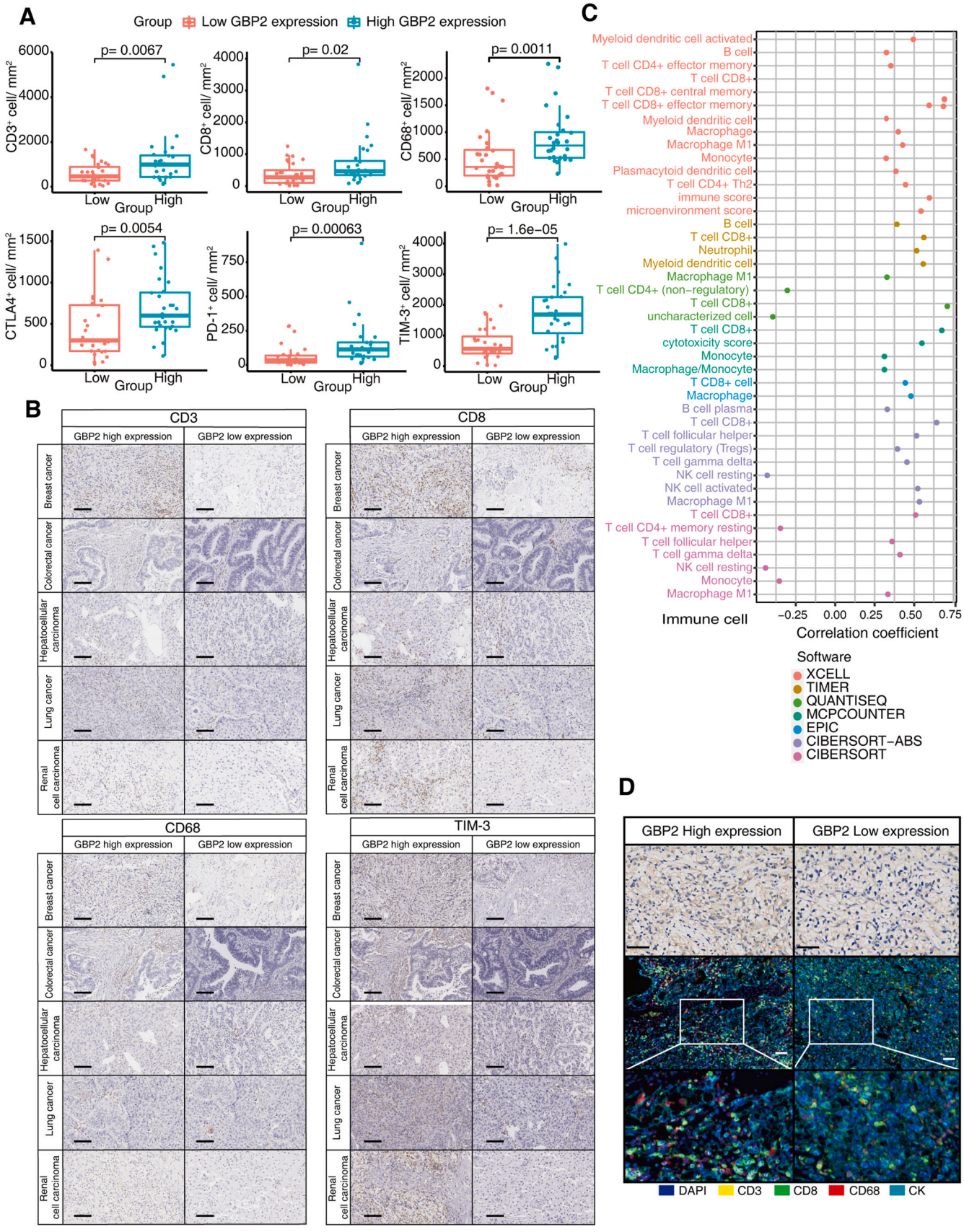

Fig. 5. GBP2 expression is correlated with immune cell infiltration in ccRCC tissues. A. The comparison of GBP2 expression and the cell densities of CD3 + , CD8 + , CD68 + , PD1 + , CTLA4 + , TIM-3 + cells in ccRCC tissues were performed and shown. B. Representative immunohistochemical staining images of CD3, CD8, CD68 and TIM-3 in patients with high GBP2 expression and low GBP2 expression were shown. Scare bar, 100 μm. C. The correlation of GBP2 expression with immune cell infiltration in TCGA ccRCC patients was determined. TCGA database was analyzed by XCELL, TIMER, QUANTISEQ, MCPCOUNTER, EPIC, CIBERSORT-ABS and CIBERSORT. D. Multiplex immunohistochemical staining using specific antibodies of CD3, CD8, CD68 and CK was performed in ccRCC tissues with high GBP2 expression and low GBP2 expression. Nave blue, nucleus; yellow, CD3 + immune cells; green, CD8 + cytotoxic T cells; red, CD68 + macrophages; pale blue, CK+ tumor cells. Scare bar, 50 μm.

proteomics is a powerful tool for screening factors that contribute to tumor growth and metastasis [25]. The CPTAC database contains a large amount of cancer proteomic data and clinical information, providing a valuable resource for biomarker discovery [16]. By integrating proteomic data from CPTAC and transcriptomic data from TCGA database, we can obtain a more comprehensive understanding of the complex regulatory mechanisms underlying cancer and identify promising biomarkers [17,26–28]. In the present study, we performed WGCNA, GO and KEGG enrichment analyses on the integrated CPTAC and TCGA data of ccRCC. We constructed a prognostic risk model consisting of five prognostic-associated proteins (GBP2, HLA-DRA, ISG15, ISG20 and ITGAX) using univariate Cox proportional hazards regression and LASSO regression analysis. This five-protein signature was found to be closely correlated with both pathological grade and clinical stage, and was able to classify ccRCC patients into low- and high-risk subgroups based on the median value of risk score. Kaplan-Meier survival analysis confirmed that the high-risk subgroup had a worse overall survival.

Among the five prognostic-associated proteins, GBP2 is an IFN-γ-induced protein that plays a critical role in host cellular immunity. Abnormal expression of GBP2 has been observed in human cancers, leading to tumor occurrence and development. For example, GBP2 enhanced the migration and invasion in breast cancer and glioma [9–12]. Consistently, our study showed that GBP2 silencing decreased the invasion and migration of ccRCC cells. Further analyses revealed that GBP2 was involved in the JAK/STAT pathway which plays crucial roles in tumor growth, metastasis, angiogenesis, and immunity [29–31]. Further investigations demonstrated that GBP2 overexpression was able to increase the phosphorylation of STAT2 and STAT3. Inhibition of JAK/STAT signaling by Ruxolitinib abolished the GBP2-promoted metastatic phenotypes.

Immune checkpoint blockade (ICB) therapy has significantly prolonged the survival of ccRCC patients. However, clinical response to ICB therapy remains unsatisfactory [32]. CD8 + cytotoxicity T lymphocytes are the primary anti-tumor immune cells that can kill tumor cells through the secretion of granzyme and perforin [33]. Recent studies have confirmed a positive correlation between GBP2 and CD8 + T cell infiltration, suggesting that GBP2 may serve as a potential immunotherapeutic target for combinatorial therapy with ICB [15]. Our study demonstrated that high GBP2 expression was associated with increased infiltration of CD8 + T lymphocytes and CD68 + macrophages in ccRCC, indicating that GBP2 may be used as a predictive factor for anti-tumor immunity in ccRCC.

5. Conclusions

In summary, we develop a prognostic risk model comprising of five hub proteins that helps to predict the prognosis and survival of ccRCC. Our data reveal strong functional correlations between GBP2 expression and tumor metastasis and immune cell infiltration in ccRCC.

Funding information

This work was supported by the National Key Research and Development Program of China (2020YFE0202200, 2017YFA0505100), the Guangdong Natural Science Foundation (2022A1515012388), the Guangdong Basic and Applied Basic Research Foundation (2022A1515111106).

CRediT authorship contribution statement

Kun Meng: Data curation, Investigation, Visualization, Writing – original draft. **Yu-Ying Li**: Formal analysis, Investigation, Visualization. **Dan-Ya Liu**: Investigation. **Li-Ling Hu**: Investigation. **Yun-Long Pan**: Supervision, Writing – review & editing. **Chris Zhiyi Zhang**: Supervision, Writing – review & editing. **Qing-Yu He**: Conceptualization, Funding acquisition, Writing – review & editing.

Declaration of Competing Interest

The authors declare that they have no known competing financial interests or personal relationships that could have appeared to influence the work reported in this paper.

Appendix A. Supporting information

Supplementary data associated with this article can be found in the online version at doi:10.1016/j.csbj.2023.04.015.

References

[1] Sung H, Ferlay J, Siegel RL, Laversanne M, Soerjomataram I, Jemal A, Bray F. Global cancer statistics 2020: GLOBOCAN estimates of incidence and mortality worldwide for 36 cancers in 185 countries. CA Cancer J Clin 2021;71(3):209–49.
[2] Xiong Y, Wang Z, Zhou Q, Zeng H, Zhang H, Liu Z, Huang Q, Wang J, Chang Y, Xia Y, Wang Y, Liu L, Zhu Y, Xu L, Dai B, Bai Q, Guo J, Xu J. Identification and validation of dichotomous immune subtypes based on intratumoral immune cells infiltration in clear cell renal cell carcinoma patients. J Immunother Cancer 2020;8(1).
[3] Wu T, Dai Y. Tumor microenvironment and therapeutic response. Cancer Lett 2017;387:61–8.
[4] Tretina K, Park ES, Maminska A, MacMicking JD. Interferon-induced guanylate-binding proteins: Guardians of host defense in health and disease. J Exp Med 2019;216(3):482–500.
[5] Quintero M, Adamoski D, Reis LMD, Ascencao CFR, Oliveira KRS, Goncalves KA, Dias MM, Carazzolle MF, Dias SMG. Guanylate-binding protein-1 is a potential new therapeutic target for triple-negative breast cancer. BMC Cancer 2017;17(1):727.
[6] Li M, Mukasa A, Inda MM, Zhang J, Chin L, Cavenee W, Furnari F. Guanylate binding protein 1 is a novel effector of EGFR-driven invasion in glioblastoma. J Exp Med 2011;208(13):2657–73.
[7] Mustafa DAM, Pedrosa R, Smid M, van der Weiden M, de Weerd V, Nigg AL, Berrevoets C, Zeneyedpour L, Priego N, Valiente M, Luider TM, Debets R, Martens JWM, Foekens JA, Sieuwerts AM, Kros JM. T lymphocytes facilitate brain metastasis of breast cancer by inducing Guanylate-Binding Protein 1 expression. Acta Neuropathol 2018;135(4):581–99.
[8] Yu X, Jin J, Zheng Y, Zhu H, Xu H, Ma J, Lan Q, Zhuang Z, Chen CC, Li M. GBP5 drives malignancy of glioblastoma via the Src/ERK1/2/MMP3 pathway. Cell Death Dis 2021;12(2):203.
[9] Nyabuto GO, Wilson JP, Heilman SA, Kalb RC, Kopacz JP, Abnave AV, Vestal DJ. The large GTPase, GBP-2, regulates rho family GTPases to inhibit migration and invadosome formation in breast cancer cells. Cancers 2021;13(22).
[10] Zhang J, Zhang Y, Wu W, Wang F, Liu X, Shui G, Nie C. Guanylate-binding protein 2 regulates Drp1-mediated mitochondrial fission to suppress breast cancer cell invasion. Cell Death Dis 2017;8(10):e3151.
[11] Yu S, Yu X, Sun L, Zheng Y, Chen L, Xu H, Jin J, Lan Q, Chen CC, Li M. GBP2 enhances glioblastoma invasion through Stat3/fibronectin pathway. Oncogene 2020;39(27):5042–55.
[12] Ren Y, Yang B, Guo G, Zhang J, Sun Y, Liu D, Guo S, Wu Y, Wang X, Wang S, Zhang W, Guo X, Li X, Li R, He J, Zhou Z. GBP2 facilitates the progression of glioma via regulation of KIF22/EGFR signaling. Cell Death Discov. 2022;8(1):208.
[13] Li R, Wang YY, Wang SL, Li XP, Chen Y, Li ZA, He JH, Zhou ZH, Li JY, Guo XL, Wang XG, Wu YQ, Ren YQ, Zhang WJ, Wang XM, Guo G. GBP2 as a potential prognostic predictor with immune-related characteristics in glioma. Front Genet 2022;13:956632.
[14] Wang J, Min H, Hu B, Xue X, Liu Y. Guanylate-binding protein-2 inhibits colorectal cancer cell growth and increases the sensitivity to paclitaxel of paclitaxel-resistant colorectal cancer cells by interfering Wnt signaling. J Cell Biochem 2020;121(2):1250–9.
[15] Wang H, Zhou Y, Zhang Y, Fang S, Zhang M, Li H, Xu F, Liu L, Liu J, Zhao Q, Wang F. Subtyping of microsatellite stability colorectal cancer reveals guanylate binding protein 2 (GBP2) as a potential immunotherapeutic target. J Immunother Cancer 2022;10(4).
[16] Whiteaker JR, Halusa GN, Hoofnagle AN, Sharma V, MacLean B, Yan P, Wrobel JA, Kennedy J, Mani DR, Zimmerman LJ, Meyer MR, Mesri M, Rodriguez H, Clinical C. Proteomic tumor analysis, A.G. Paulovich, CPTAC Assay Portal: a repository of targeted proteomic assays. Nat Methods 2014;11(7):703–4.
[17] Hutter C, Zenklusen JC. The cancer genome atlas: creating lasting value beyond its data. Cell 2018;173(2):283–5.
[18] Langfelder P, Horvath S. WGCNA: an R package for weighted correlation network analysis. BMC Bioinforma 2008;9:559.
[19] Subramaniana A, Tamayo P, Mootha VK, Mukherje S, Ebert BL, et al. Gene set enrichment analysis: A knowledge-based approach for interpreting genome-wide expression profiles. PNAS 2005;102:15545–50.
[20] Wiśniewski JR, Zougman A, Nagaraj N. Mann M.Universal sample preparation method for proteome analysis. Nat Methods 2009;6:359–62.

[21] Liu B, Huang R, Fu T, He P, Du C, Zhou W, Xu K, Ren T. GBP2 as a potential prognostic biomarker in pancreatic adenocarcinoma. PeerJ 2021;9:e11423.
[22] Warde-Farley D, Donaldson SL, Comes O, Zuberi K, Badrawi R, Chao P, Franz M, Grouios C, Kazi F, Lopes CT, Maitland A, Mostafavi S, Montojo J, Shao Q, Wright G, Bader GD, Morris Q. The GeneMANIA prediction server: biological network integration for gene prioritization and predicting gene function (Web Server issue). Nucleic Acids Res. 2010;38:W214–20.
[23] Fassan M, Cavallin F, Guzzardo V, Kotsafti A, et al. PD-L1 expression, CD8+ and CD4+ lymphocyte rate are predictive of pathological complete response after neoadjuvant chemoradiotherapy for squamous cell cancer of the thoracic esophagus. Cancer Med 2019;8(13):6036–48.
[24] Fu T, Dai LJ, Wu SY, Xiao Y, Ma D, Jiang YZ, Shao ZM. Spatial architecture of the immune microenvironment orchestrates tumor immunity and therapeutic response. J Hematol Oncol 2021;14(1):98.
[25] Kowalczyk T, Ciborowski M, Kisluk J, Kretowski A, Barbas C. Mass spectrometry based proteomics and metabolomics in personalized oncology. Biochim Biophys Acta Mol Basis Dis 2020;1866(5):165690.
[26] Rappoport N, Shamir R. Multi-omic and multi-view clustering algorithms: review and cancer benchmark. Nucleic Acids Res 2018;46(20):10546–62.
[27] Xiao Y, Bi M, Guo H, Li M. Multi-omics approaches for biomarker discovery in early ovarian cancer diagnosis. EBioMedicine 2022;79:104001.
[28] Menyhart O, Gyorffy B. Multi-omics approaches in cancer research with applications in tumor subtyping, prognosis, and diagnosis. Comput Struct Biotechnol J 2021;19:949–60.
[29] Hu X, Li J, Fu M, Zhao X, Wang W. The JAK/STAT signaling pathway: from bench to clinic. Signal Transduct Target Ther 2021;6(1):402.
[30] Villarino AV, Kanno Y, O'Shea JJ. Mechanisms and consequences of Jak-STAT signaling in the immune system. Nat Immunol 2017;18(4):374–84.
[31] Villarino AV, Gadina M, O'Shea JJ, Kanno Y. SnapShot: Jak-STAT signaling II. Cell 2020;181(7):1696–1696 e1.
[32] Krishna C, DiNatale RG, Kuo F, Srivastava RM, Vuong L, Chowell D, Gupta S, Vanderbilt C, Purohit TA, Liu M, Kansler E, Nixon BG, Chen YB, Makarov V, Blum KA, Attalla K, Weng S, Salmans ML, Golkaram M, Liu L, Zhang S, Vijayaraghavan R, Pawlowski T, Reuter V, Carlo MI, Voss MH, Coleman J, Russo P, Motzer RJ, Li MO, Leslie CS, Chan TA, Hakimi AA. Single-cell sequencing links multiregional immune landscapes and tissue-resident T cells in ccRCC to tumor topology and therapy efficacy. Cancer Cell 2021;39(5):662–677 e6.
[33] Golstein P, Griffiths GM. An early history of T cell-mediated cytotoxicity. Nat Rev Immunol 2018;18(8):527–35.